PERGAMON

International Journal of Multiphase Flow 26 (2000) 1095–1115

International Journal of Multiphase Flow

www.elsevier.com/locate/ijmulflow

A steady state, one dimensional, model for boiling two phase flow in triangular micro-channel

Y.P. Peles*, S. Haber

Department of Mechanical Engineering, Technion—Israel Institute of Technology, Haifa, Israel

Received 23 March 1998; received in revised form 11 July 1999

Abstract

The potential advantages of triangular micro-channels incorporated into heat generating small devices are discussed. A simple one dimensional model of boiling two-phase flow and heat transfer in a single triangular micro-channel is investigated. The flow of the liquid phase inside the micro-channels is driven by surface tension and friction forces that exist at the interface between the fast moving vapor and liquid. The flow of the vapor phase is controlled by the heat flux generated and removed from the device. As the liquid flows through the channel it evaporates, its cross-section diminishes and the radius of curvature at the liquid vapor interface decreases. Thus, according to Young–Laplace equation, the liquid–vapor pressure difference increases along the channel. Consequently, a large decrease in the liquid pressure along the channel is obtained if the vapor pressure remains almost uniform. That pressure drop in the liquid phase is responsible for the onset of liquid flow. Along the micro-channel the increasing amount of generated vapor causes vapor velocity to increase and friction forces exerted on the liquid phase become significant until dry-out occurs. Since in the dry-out zone the heat transfer is drastically diminished, dry-out length estimates are of major concern in micro-channel design. A solution of a first order non-linear differentiated equation is required to predict dry-out lengths and their dependence on the dimensionless parameters governing the flow. A numerical simulation was carried out for the case of water flowing in a vertical channel of equilateral triangular cross-section. Hydraulic diameters from 0.1 to 1 mm, heat fluxes from 10 to 600 W/cm^2 and contact angles of 5° to 40° were assumed. The results validate the basic assumption that vapor pressure along the micro-channel is almost uniform. In many practical applications the differential equation can be simplified and solved analytically and the dry-out length are determined via a solution of an algebraic equation. Finally, it was demonstrated that the dry-out lengths seem to fit the dimensions of microelectronic devices.

Keywords: Micro-channel; Dry-out length; Boiling two-phase flow

* Corresponding author.

PII: S0301-9322(99)00084-1

1. Introduction

The reduction in size of electronic devices and the reduction in transistor rise time poses a formidable challenge to the packaging community. To facilitate effective, near term utilization of the future chips, the design and performance of first and second level packaging will need to improve dramatically relative to the current state-of-the- art. Chip heat fluxes exceeding 100 W/cm^2 are expected by the year 2000 (Jacobs and Hartnett, 1991). Because of the high localized heat fluxes, the temperature uniformity of the chip surface is also an important consideration in determining the type of the heat rejection system to be used. For this reason, micro-channels, in which liquid flows and evaporates, may be a promising alternative cooling scheme. Recent development in the semiconductor technology have made extraordinary advances in device construction and miniaturization. Those developments allow the manufacturing of micro heat exchangers ranging from 10 to 1000 μm.

In the earliest research on micro-scale flow and heat transfer, Tuckermann and Pease (1981, 1982) studied the single phase fluid flow and heat transfer characteristics in micro-channels, and demonstrated that electronic chips can effectively be cooled by means of forced convection flow of water through micro channels. Their result confirm the possibility of using forced convection flow in micro-channels for electronic chips and devices.

Wu and Little (1983, 1984) measured the flow friction and heat transfer of gases flowing through micro-channels and observed that the convective heat transfer characteristics depart from typical thermofluid experimental results, obtained previously for conventional size channels. Several other investigation (Pfahler et al., 1990, 1991; Peng et al., 1994; Cho et al., 1991) have found similar anomalous behavior. An extensive review of the available single phase micro-channel cooling data has been done by Bailley et al. (1995). Although single phase micro-channel flow can effectively cool miniature devices, it presents some inherent disadvantages such as large pressure drops and stream-wise increase in the heat sink temperature. On the other hand, boiling two phase flow can achieve very high heat fluxes for constant flow rates, while maintaining a relatively constant temperature.

Bowers and Mudawar (1994a) performed an experimental study of flow boiling with R-113 in circular mini-channels ($D = 2.54$ mm) and micro-channels ($D = 510$ μm) heat sinks and demonstrated that high values of heat fluxes can be achieved. Bowers and Mudawar (1994b) also modeled the pressure drop, in micro-channels and mini-channels, using Collier (1981) and Wallis (1969) homogeneous equilibrium model, who assumed that the liquid and vapor phases possess uniform properties and form a homogeneous mixture with equal and uniform velocity.

Landram (1994) developed an analytical model for two-phase boiling heat transfer in a rectangular micro-channel having high aspect ratio. Initially, the flow regimes in the channel were mapped, than the heat transfer and wall temperature were evaluated, based on a heat transfer coefficient quoted in the literature.

A different analytical approach to the pressure drop in boiling two-phase flow in extremely narrow channels (35–110 μm between plates) was suggested by Moriyama et al. (1992). The model assumes an equal and constant liquid film thickness on the upper and lower wall. The momentum equation for the liquid and vapor phases was introduced in order to evaluate the pressure drop along the gap for slug flow and the film flow regimes. Peng et al. (1998) argued

that boiling nucleation in micro channels is much more difficult to achieve than in conventional size channels.

Cotter (1984) was the first to point out the advantages of using a non-circular micro-channel as a micro heat pipe. The micro-heat pipe makes use of the sharp-angled corner region of the channel as liquid arteries. As the liquid progresses along the channel, it contains less liquid, and has a smaller radius of curvature at the liquid–vapor interface, and hence has a depressed liquid pressure. The pressure difference is responsible for both the liquid and vapor flows. Following Cotter, Peterson et al. (1993) investigated experimentally the thermal behavior of arrays of micro heat pipes, fabricated in a silicon wafer, and indicated that incorporating an array of micro heat pipes as an integral part of semiconductors devices could significantly improve the thermal performance. Finally, Longtin et al. (1994) developed a one dimensional model of the evaporation and adiabatic section to yield pressure, velocity, and film thickness along the length of a micro heat pipe having an equilateral triangle cross section.

Although past research have focused on the mechanism governing heat transfer and fluid flow in micro-channels, none has investigated the advantage inherit by non circular geometry, that is used in micro heat pipes. In the present investigation, a one dimensional model of boiling two phase fluid flow and heat transfer in a triangular micro channel has been developed, and solved numerically. The results demonstrated that a self-sustained flow could be achieved in micro-channels possessing triangular cross-section and that the evaporation region along the micro-channel can be sufficiently long, sustaining a low and constant temperature along a high heat generating devices such as found in microelectronics.

2. Micro-channel flow model

A model is developed to predict the boiling two-phase flow in a triangular micro-channel. The model is one dimensional and considers only axial variation along the channel. The conservation of mass, energy and the Young–Laplace equation (for the interface between the vapor and the liquid domains), are introduced into the momentum equation to form a first order differential equation for the liquid domain, and an algebraic equation for the vapor domain. Boundary conditions are then applied to achieve closure of the equations. The resulting differential equation are solved numerically to yield the liquid radius of curvature, the effective dry-out length, velocity, pressure, and film thickness as a function of the hydraulic diameter of the channel, and the thermophysical properties of the working fluid.

The channel cross-section is an equilateral triangle (see Fig. 1). When heat is added to the flow, the radius of curvature of the liquid–vapor meniscus decreases gradually along the channel, thus decreasing the liquid pressure and generating a capillary driving pressure. As a first approximation, that is posteriorily validated, the vapor pressure can be considered constant along the channel, since in many practical cases the vapor pressure drop is very small compared with that of the liquid pressure drop.

For the present model, the following assumption have been made: the flow is laminar, incompressible, steady with constant properties and contact angle, the heat flux along the channel is uniform and the vapor velocity at any x location is much higher than the liquid velocity. The radius of curvature parallel to the channel axis is much larger than that normal

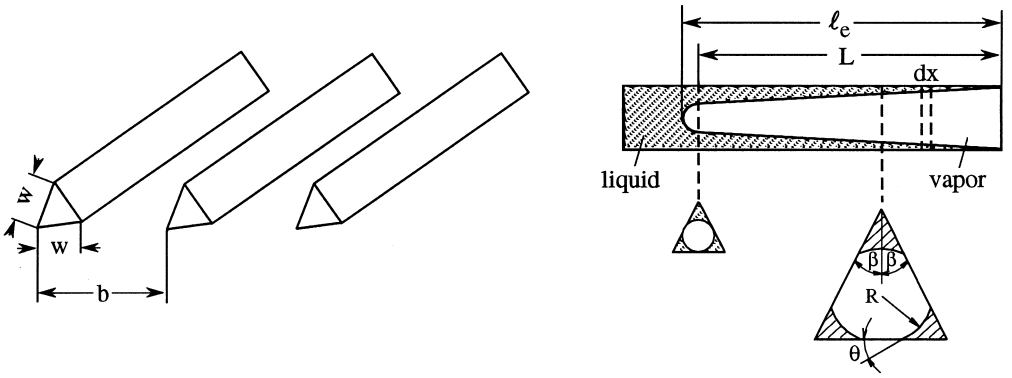

Fig. 1. The micro-channel heat exchanger consists of micro-channels of triangular cross-section filled with the liquid and vapor phases.

to the channel and may change along the channel. Thus, the mean radius of curvature is approximately equal to the radius of curvature normal to the channel axis. The evaporation occurs, mostly, when the liquid occupies the corners of the triangle, while the vapor has a common interface with the solid wall ($L/l_e \cong 1$ in Fig. 1), and evaporation is the sole effect, caused by heating. This requires that vapor temperature variations, during evaporation, is small.

Secondary flows that normally exist in triangular channels are averaged out in our simple one-dimensional model. Since these flows are small in magnitude, the pressure difference within the liquid cross-section is small and consequently a uniform pressure within the liquid cross-section can be assumed.

3. Vapor domain

The vapor cross-section can be assumed to be approximately constant (see Fig. 2). Energy input into the control volume results in vaporization of the liquid at the interface. Since the vapor temperature is assumed constant, and the heat flux is uniform, the vapor input along the channel is constant. Thus the energy equation becomes:

$$Qbx = \dot{m}_G \lambda \tag{1}$$

where Q is the heat flux, b is the distance between adjacent channels (see Fig. 1), $\dot{m}_G$ is the vapor mass flow rate, and λ is the latent heat of vaporization. Henceforth, we shall use the suffix G or/and L to denote vapor or/and liquid variables.

The momentum equation for the vapor is:

$$\frac{d(\rho_G v_G^2 A_G)}{dx} = -A_G \frac{dp_G}{dx} - (S_{GW}\tau_{GW} + S_{GL}\tau_{GL}) \tag{2a}$$

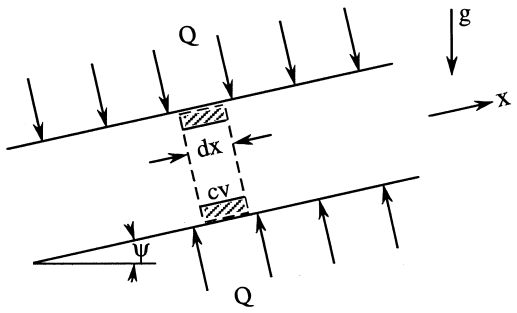

Fig. 2. The control volume.

where S_{GL} and S_{GW} denote the respective vapor–iquid and the respective vapor–wall interface length measured at a specific cross-section. τ_{GL} and τ_{GW} stand for the shear stresses at the vapor–liquid and the vapor–wall interfaces, respectively.

Since the vapor velocity is much larger than that of the liquid $\tau_{GL} \approx \tau_{GW}$ and Eq. (2a) can be simplified as follows:

$$\frac{d(\rho_G v_G^2 A_G)}{dx} = -A_G \frac{dp_G}{dx} - S_G \tau_G \tag{2b}$$

where S_G, A_G, P_G, ρ_G, v_G and τ_G are the perimeter, cross-section area, pressure, density, velocity, and shear stress at the vapor boundaries, respectively.

The hydraulic diameter of the vapor phase is:

$$D_{hG} = \frac{4A_G}{S_G} \tag{3}$$

and the vapor velocity v_G is obtained from the mass conservation equation:

$$v_G = \frac{\dot{m}_G}{\rho_G A_G}. \tag{4}$$

Since the Reynolds number is very small, the flow is laminar and the shear stress at the perimeter can be expressed by:

$$\tau_G = \frac{\rho_G v_G^2 \xi_G}{2} \tag{5}$$

where ξ_G is the vapor friction factor. Introducing Eqs. (3)–(5) into the momentum equation (2b) yields:

$$\frac{2\dot{m}_G}{\rho_G A_G^2}\frac{d\dot{m}_G}{dx} - \frac{\dot{m}_G^2}{\rho_G A_G^3}\frac{dA_G}{dx} = -\frac{dp_G}{dx} - \frac{2\dot{m}_G \mu_G}{D_{hG}^2 \rho_G A_G}(\xi Re)_G \tag{6a}$$

Posteriorily it is shown that the variation of A_G along x is quite small and the contribution of

the second term on the LHS of Eq. (6a) is small compared with that of the first term. Thus, Eq. (6a) can further be simplified as follows:

$$\frac{2\dot{m}_G}{\rho_G A_G^2}\frac{d\dot{m}_G}{dx} = -\frac{dp_G}{dx} - \frac{2\dot{m}_G\mu_G}{D_{hG}^2\rho_G A_G}(\xi Re)_G \tag{6b}$$

where the Reynolds number is:

$$Re_G = \frac{v_G D_{hG}\rho_G}{\mu_G}. \tag{7}$$

Using Eq. (1), the momentum equation becomes:

$$\frac{dp_G}{dx} = -\left[\frac{2bQ\mu_G}{\lambda D_{hG}^2\rho_G A_G}(\xi Re)_G + \frac{2Q^2b^2}{\rho_G A_G^2\lambda^2}\right]x. \tag{8}$$

For laminar flows the term $(\xi Re)_G$ depends on the cross-section geometry but not on x. Since $(\xi Re)_G$ varies from nearly 13.3 for triangular cross-section (Bejan, 1984) to approximately 16 for circular cross-section, the value of 14.7 is used in our case for the cross-section of the vapor domain. Integrating Eq. (8) the pressure is expressed by:

$$p_G = -\left[\frac{14.7bQ\mu_G}{\lambda D_{hG}^2\rho_G A_G} + \frac{Q^2b^2}{\rho_G A_G^2\lambda^2}\right]x^2 + p_{G0} \tag{9}$$

where p_{G0} is the vapor pressure at $x = 0$.

For example, for water at 100°C, a channel hydraulic diameter of 200 μm, $b = 2D_{hG}$, and heat flux of 10 W/cm^2, the pressure drop along a channel 1 cm long is $\Delta p = 6.1$ Pa. This is much smaller than the pressure drop expected in the liquid domain (about one bar). In many practical cases (as shall later be shown in chapter 7) the vapor pressure drop is much smaller than the liquid pressure drop. Consequently, the pressure in the vapor phase can be assumed to remain constant. Thus, the liquid pressure drop can be determined by applying the Laplace–Young equation at the liquid–vapor meniscus.

4. Liquid domain

Conservation of mass and momentum of the liquid phase that occupies a control volume bounded by two finite cross-sectional areas across the micro-channel, dx apart (see Fig. 3a) yields:

$$\int_V \rho_L g_x \, dV + \int_S (T \cdot dS)_x = \int_S \rho_L v_x(\bar{v} \cdot \bar{n}) \, ds \tag{10}$$

where ρ_L is the liquid density, g_x is the gravity in x direction, T is the stress tensor and S stands for the surface area bounding the control volume. We shall, henceforth, address each term in Eq. (10) separately. The contribution of the surface forces $\int_S (T \cdot dS)$ can be written in

the following form:

$$\int_S T \cdot \, \mathrm{d}S = I - D + F \tag{11}$$

where I stands for the contribution of the pressure at the liquid interfaces, D is the contribution of the wall–liquid friction force, and F reflects the contribution of the liquid–vapor friction force.

The pressure contribution along x is (using the relation $\mathrm{dA_G} = -\mathrm{dA_L}$):

$$I = -p_{\mathrm{L}} A_{\mathrm{L}}|_{x+\mathrm{d}x} - p_{\mathrm{L}} \mathrm{d}A_G + .p_{\mathrm{L}} A_{\mathrm{L}}|_x = -A_{\mathrm{L}} \mathrm{d}p_{\mathrm{L}}. \tag{12}$$

The Young–Laplace equation is:

$$p_{\mathrm{G}} - p_{\mathrm{L}} = \sigma\left(\frac{1}{R} + \frac{1}{R_2}\right) \cong \frac{\sigma}{R} \tag{13}$$

where R is the radius of curvature normal to the x direction. Here, the radius of curvature parallel to the x direction (R_2) is much larger than R, and therefore $1/R_2$ was neglected. Thus, Eq. (12) possesses the following form:

$$I = -A_{\mathrm{L}} d\left(p_{\mathrm{G}} - \frac{\sigma}{R}\right) \tag{14}$$

and since the surface tension is assumed constant and $\mathrm{p_G} \approx$ constant :

$$I = A_{\mathrm{L}} \sigma \mathrm{d}\left(\frac{1}{R}\right). \tag{15}$$

The wall–liquid friction force (Fig. 3b) is:

$$D = \tau_{\mathrm{LW}} S_{\mathrm{LW}} \, \mathrm{d}x \tag{16}$$

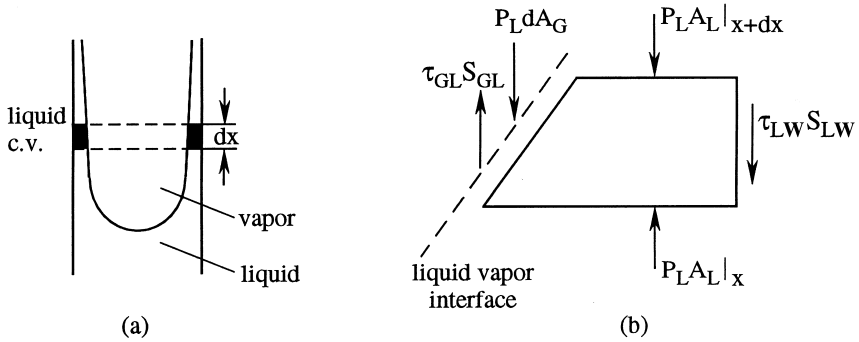

Fig. 3. Forces exerted on the liquid control volume.

where S_{LW} is the liquid–wall interface length. The shear stress can be expressed in the following form:

$$\tau_{LW} = \frac{1}{2}\rho_L v_L^2 \xi_L \tag{17}$$

where ξ_L is the liquid friction factor:

$$\xi = \frac{k}{Re_L} \tag{18}$$

and Re_L is the liquid Reynolds number based on liquid–wall hydraulic diameter, and $k = 13.3$ for triangular duct geometry, as previously noted.

Substituting Eqs. (17) and (18) into (16) and utilizing equations similar to Eqs. (3) and (4) for the liquid phase, the wall–liquid friction force is:

$$D = 2k\frac{\dot{m}_L}{\rho_L}\frac{\mu_L}{D_{hL}^2}\mathrm{d}x. \tag{19}$$

The vapor–liquid friction force (Fig. 3b) is:

$$\tau_{GL}\mathrm{d}A_{GL} = \tau_{GL}S_{GL}\,\mathrm{d}x. \tag{20}$$

As discussed previously τ_{GL} can be expressed as:

$$\tau_{GL} = \xi_G\frac{1}{2}\rho_G v_G^2. \tag{21}$$

Inserting Eq. (21) into Eq. (20) and using Eqs. (1), (4) and (7) yields:

$$F = \tau_{GL}\,\mathrm{d}A_{GL} = (\xi Re)_G\frac{Qbx}{2\lambda\rho_G A_G}\frac{\mu_G}{D_{hG}}S_{GL}\,\mathrm{d}x. \tag{22}$$

The momentum of the fluid along x in Eq. (10) is (Fig. 4):

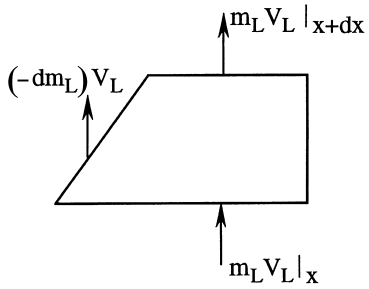

Fig. 4. Momentum flux through the liquid control volume.

$$\mathrm{d}M = \int_S \rho_L v_L (\bar{v}_L \cdot \bar{n})\, \mathrm{d}S = \dot{m}_L dv_L = d(\dot{m}_L v_L) - v_L d\dot{m}_L. \tag{23}$$

However, from the energy equation:

$$\dot{m}_L = \frac{Qb}{\lambda} L - \dot{m}_G = \frac{Qb}{\lambda}(L - x) \tag{24}$$

where L is the dry-out length which is yet unknown.

Introducing Eq. (4) for the liquid domain and Eq. (24) into (23) yields:

$$dM = \frac{Q^2 b^2}{\lambda^2 \rho_L} d\left[\frac{(L-x)^2}{A_L}\right] + \frac{Q^2 b^2 (L-x)}{\lambda^2 \rho_L A_L} \mathrm{d}x. \tag{25}$$

The gravity force component along x is:

$$\int_V \rho_L g_x \, \mathrm{d}V = \rho_L g A_L \sin\psi \, \mathrm{d}x \tag{26}$$

where ψ is the inclination angle of the gravity acceleration vector (see Fig. 2).

Form geometrical consideration, the following relations can be found:

$$A_L = C_1 R^2 \tag{27}$$

$$D_{hL} = C_2 R \tag{28}$$

$$S_{GL} = C_3 R \tag{29}$$

where:

$$C_1 = 3\left[\cos^2(\beta+\theta) - \frac{\pi}{4} + \frac{\beta+\theta}{2} + \frac{\cos(\beta+\theta)}{2}\right] \tag{30}$$

$$C_2 = \frac{2C_1 \sin\beta}{3\cos(\beta+\theta)} \tag{31}$$

$$C_3 = \frac{\pi}{2} - (\beta+\theta) \tag{32}$$

where θ is the contact angle and β is half included angle ($\beta = \pi/6$ for an equilateral triangle).

The contact angle dependence on the parameters of the problem such as materiel composition of the liquid and the wall, temperature, etc. Since the vapor pressure was shown to remain almost constant, the evaporation temperature is uniform over the whole solution domain, and consequently the contact angle can be assumed to remain constant along x, for a given set of working parameters.

Introducing Eqs. (15), (19) and (22) into Eq. (11), introducing Eqs. (11), (25) and (26) into (10), and using relation (30)–(32) the momentum equation possesses the following form:

$$-\sigma C_1\frac{\mathrm{d}R}{\mathrm{d}x}+\frac{2Q^2b^2}{\lambda^2\rho_{\mathrm{L}}C_1}\frac{(L-x)^2}{R^3}\frac{\mathrm{d}R}{\mathrm{d}x}=\rho_{\mathrm{L}}gC_1\sin\psi R^2 + \frac{2kQb\mu_{\mathrm{L}}}{\lambda\rho_{\mathrm{L}}C_2^2}\frac{(L-x)}{R^2}-(\xi Re)_{\mathrm{G}}\frac{Qb\mu_{\mathrm{G}}}{2\lambda\rho_{\mathrm{G}}}\frac{C_3}{A_{\mathrm{G}}D_{\mathrm{hG}}}xR+\frac{Q^2b^2}{\lambda^2\rho_{\mathrm{L}}C_1R^2}(L-x). \tag{33}$$

A non-dimensional form of Eq. (33) is:

$$\frac{\mathrm{d}\bar{R}}{\mathrm{d}\bar{x}}\left[2\pi_1\frac{(\bar{L}-\bar{x})^2}{\bar{R}^3}-1\right]=\pi_2\bar{R}^2-\pi_3\bar{x}\bar{R}+(\pi_1+\pi_4)\frac{(\bar{L}-\bar{x})}{\bar{R}^2} \tag{34}$$

where:

$$\bar{R}=\frac{R}{\mathrm{D}_{hG}};\quad \bar{x}=\frac{x}{D_{\mathrm{hG}}};\quad \bar{L}=\frac{L}{D_{\mathrm{hG}}} \tag{35a}$$

$$\pi_1=\frac{Q^2b^2}{\lambda^2\rho_{\mathrm{L}}C_{\mathrm{L}}^2\sigma D_{\mathrm{hG}}}\ \text{(non-dimensional momentum flux)}$$

$$\pi_2=\frac{\rho_{\mathrm{L}}gD_{\mathrm{hG}}^2\sin\psi}{\sigma}\ \text{(non-dimensional body forces)}$$

$$\pi_3=(\xi Re)_{\mathrm{G}}\frac{Qb\mu_{\mathrm{G}}D_{\mathrm{hG}}C_3}{2\lambda\rho_{\mathrm{G}}\sigma A_{\mathrm{G}}C_1}\ \text{(non-dimensional vapor–liquid friction forces)}$$

$$\pi_4=\frac{2kQb\mu_{\mathrm{L}}}{\sigma\lambda\rho_{\mathrm{L}}D_{\mathrm{hG}}C_1C_2^2}\ \text{(non-dimensional wall–liquid friction forces)} \tag{35b}$$

It should be noted that the capillary force is introduced by the multiplier -1 of $\mathrm{d}\bar{R}/\mathrm{d}\bar{x}$.

5. Boundary condition

Eq. (34) is a first order, nonlinear differential equation. If $\bar{L}$ is known, $\bar{R}$ is the only unknown, and a single boundary condition is required to solve Eq. (34). However, the dry-out length $\bar{L}$ is a-priori unknown and an additional condition (say at $\bar{X}=\bar{L}$) is needed.

The solution commences at the point where the liquid divides into three separate segments (i.e. $L/l_{\mathrm{e}}\cong 1$ in Fig. 1). Thus, the initial boundary condition for the radius of curvature at $x=0$ based on the average vapor hydraulic diameter is: $R(x=0)=\frac{0.53D_{\mathrm{h}}}{\cos(\beta+\theta)}$ or in dimensionless form: $\bar{R}(\bar{x}=0)=\frac{0.53}{\cos(\beta+\theta)}$. The second condition stems from the fact that the liquid pressure reduces almost to zero at $\bar{x}=\bar{L}$, since $\bar{R}(\bar{x}=\bar{L})\approx\frac{\sigma}{P_{\mathrm{G}}D_{\mathrm{hG}}}$, where P_{G} is the vapor pressure.

The position of the vapor initial cross section ($x=0$) with respect to the liquid outside level is obtained by the following expression:

$$h(x=0)=\frac{4\sigma\cos(\theta)}{\rho g D_{\mathrm{h}}} \tag{36}$$

where $h(x=0)$ is the vapor inlet cross section with respect to the liquid level outside the channel. Eq. (36) results from the equilibrium between the hydrostatic pressure and the capillary pressure at $x=0$:

$$\rho g h=\left[P_{\mathrm{amb}}-P_{\mathrm{L}}(x=0)\right]=\frac{4\sigma\cos(\theta)}{D_{\mathrm{h}}} \tag{37}$$

where P_{amb} is the liquid pressure outside the channel.

6. Numerical procedure

Eq. (34) together with the initial boundary conditions ($\bar{X}=0$) was numerically solved applying fourth-order Runge–Kutta ODE method. An iterative procedure was carried out, in order to meet the second boundary condition at $\bar{x}=\bar{L}$.

The solving procedure consist of the following consecutive steps:

1. Choose the dimensional parameters, and calculate the dimensionless parameters defined in Eqs. (35a) and (35b).
2. Assume the dry-out length ($\bar{L}$) for the first iteration.
3. Solve Eq. (34) and find $\bar{R}_1$ at $\bar{x}=\bar{L}$ where $\bar{R}_1$ is the calculated radius of curvature at dry-out after a first iteration.
4. If

$$\left|\frac{\bar{R}(\bar{x}=\bar{L})-\bar{R}_1(\bar{x}=\bar{L})}{\bar{R}(\bar{x}=\bar{L})}\right|>\mathrm{ERROR}$$

and

(a) $R_i(\bar{x}=\bar{L})$, $R_{i-1}(\bar{x}=\bar{L})>R(\bar{x}=\bar{L})$ then $\bar{L}=\bar{L}+d\bar{L}$.
(b) $R_i(\bar{x}=\bar{L})>R(\bar{x}=\bar{L})$ and $R_{i-1}(\bar{x}=\bar{L})<R(\bar{x}=\bar{L})$ then: $\mathrm{d}\bar{L}=\mathrm{d}\bar{L}/2$, $\bar{L}=\bar{L}+\mathrm{d}\bar{L}$
(c) $R_i(\bar{x}=\bar{L})$, $R_{i-1}(\bar{x}=\bar{L})<R(\bar{x}=\bar{L})$ then $\bar{L}=\bar{L}-\mathrm{d}\bar{L}$.
(d) $R_i(\bar{x}=\bar{L})<R(\bar{x}=\bar{L})$ and $R_{i-1}(\bar{x}=\bar{L})>R(\bar{x}=\bar{L})$ then: $\mathrm{d}\bar{L}=\mathrm{d}\bar{L}/2$, $\bar{L}=\bar{L}-\mathrm{d}\bar{L}$.
go back to step 2 using the newly predicted dry-out length.

5. Calculate v_{L}, A_{L}, P_{L}

A uniform grid was used with 100 grid points. The numerical solution was found to be essentially independent of the number of grid points for a large number of points.

7. Result and discussion

The mathematical model can be used to predict the following:

- The dependence of the dry-out length on the thermophysical properties of the working fluid, the heat flux, channel hydraulic diameter, and contact angle.
- The radius of curvature, the pressure, and velocity distribution along the channel.

The numerical solution of Eq. (34) was carried out for dimensions and fluids normally used to cool microelectronics devices e.g. water evaporating in an vertical micro- channel at various hydraulic diameters (100 μm $< D_{hG} <$ 1000 μm), heat fluxes (10 W/cm^2 $< Q <$ 600 W/cm^2), and contact angle ($5^\circ < \theta < 40^\circ$).

The following additional nondimensionalizations are employed:

$$\bar{P}_L = \frac{P_L}{P_G} = 1 - \frac{\sigma}{P_G R}; \quad \bar{A}_L = \frac{A_L}{A_L(x=0)} = \frac{\bar{R}^2}{\bar{R}^2(\bar{x}=0)};$$

$$\bar{v} = \frac{v}{v(x=0)} = \frac{\bar{L}-\bar{x}}{\bar{L}} \frac{\bar{R}^2(x=0)}{\bar{R}^2}.$$

Fig. 5 shows the dependence of the radius of curvature on axial position given that the working fluid is water, $Q = 10$ W/cm^2, $D_{hG} = 300$ μm and $\theta = 5.4^\circ$. The radius of curvature is monotonically decreasing along the channel due to water evaporation, and hence the water cross-section decreases sharply along the channel (see Fig. 6) causing the velocity to increase (see Fig. 7) so that mass balance is maintained. Near the end of the evaporation region the radius of curvature $\bar{R}$ and the cross section are small. For constant heat flux $\bar{R}$ (and the cross section) must decrease sharply due to liquid evaporation, causing the velocity to increase sharply.

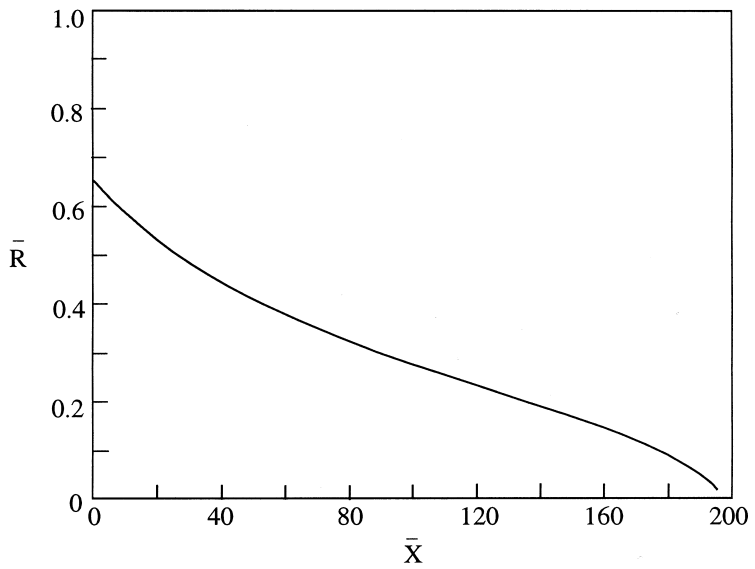

Fig. 5. Dimensionless radius of curvature versus axial position for $D_{hG} = 300$ μm, $Q = 10$ W/cm^2 and different angles.

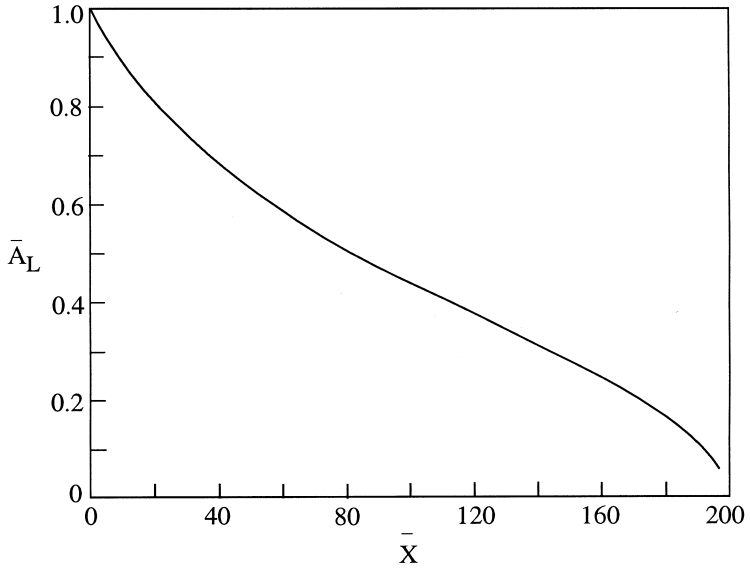

Fig. 6. Dimensionless liquid cross section versus axial position for $D_{hG} = 300$ μm, $Q = 10$ W/cm^2 and contact angle $\theta = 5.4°$.

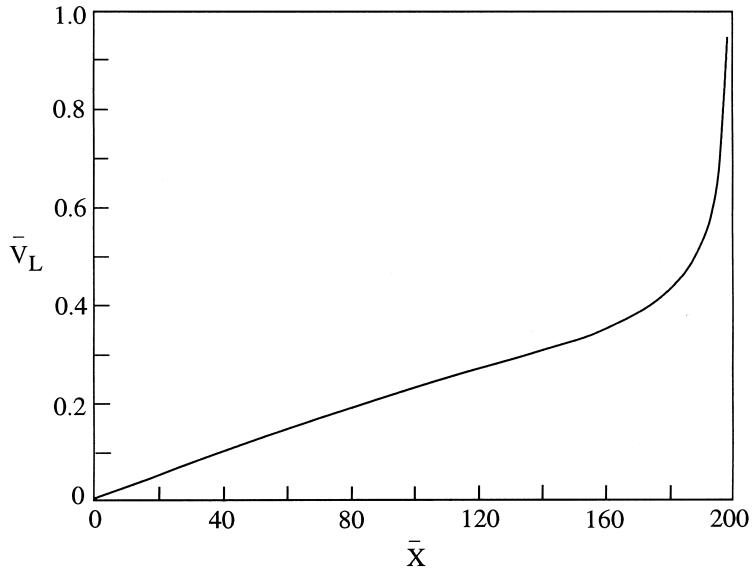

Fig. 7. Dimensionless liquid velocity versus axial position for $D_{hG} = 300$ μm, $Q = 10$ W/cm^2 and contact angle $\theta = 5.4°$.

Since the radius of curvature decreases along the channel, and the vapor pressure does not change significantly, the liquid pressure decreases along the evaporation region (see Fig. 8). A sharp drop takes place near the end of the evaporation region. It implies that the dry-out $\bar{L}$ is almost insensitive to the pressure values at $\bar{x} = \bar{L}$. For $\bar{P}(\bar{x} = \bar{L}) < 0.9$ the dry-out length would practically be unaltered.

Fig. 9 shows the dependence of different terms of Eq. (34), for water at $Q = 10$ W/cm^2, $D_{hG} = 300$ μm, and a contact angle of 5.4°. It is shown that in this case all terms in Eq. (34) are of the same order except for the much smaller term representing the momentum flux. It can be seen that different forces control the evaporation domain as x increases. For small x's capillary forces and body forces are significant while for $\bar{x} \approx 0.5\bar{L}$, capillary forces, friction forces at the wall, and the friction forces at the vapor interface, control the flow. For large x's ($x \approx L$) capillary forces and friction forces at the wall are significant while other forces become negligible. Since the liquid velocity increases sharply along the channel, the wall-liquid friction forces in Eq. (34), represented by the term $\pi_4((\bar{L} - \bar{x})/\bar{R}^2)$, increases monotonously along the channel. The vapor velocity at low x values is low, since only a small portion of the total heat is added to evaporate the liquid. A constant heat flux along the channel causes a constant liquid evaporation, and since the vapor cross section is nearly constant, the vapor velocity increases sharply with x for small values of x. As x increases the radius of curvature reduces slowly, hence, the contribution of liquid–vapor friction forces in Eq. (34) ($\pi_3 \bar{x}\bar{R}$) increases. At high values of x, the vapor velocity increases slowly and the radius of curvature decreases sharply, thus the contribution of the liquid–vapor friction forces decreases. The body force term ($\pi_2 \bar{R}^2$) decreases monotonously, since the liquid volume decreases as x increases. The non dimensional number π_1 is much smaller than 1, and $\pi_1 \ll \pi_4$, thus, Eq. (34) can be rewritten,

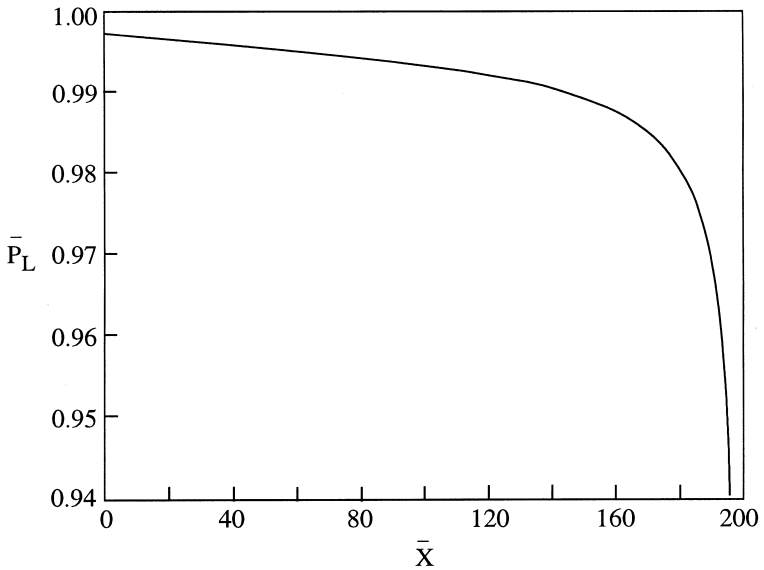

Fig. 8. Dimensionless liquid pressure versus axial position for $D_{hG} = 300$ μm, $Q = 10$ W/cm^2 and contact angle $\theta = 5.4°$.

for water evaporating in a micro-channel of hydraulic diameter of the order of 10^{-4} m and heat flux of the order of 10 W/cm^2, as:

$$\frac{d\bar{R}}{d\bar{x}} = -\pi_2\bar{R}^2 + \pi_3\bar{x}\bar{R} - \pi_4\frac{(\bar{L}-\bar{x})}{\bar{R}^2} \tag{38}$$

As the hydraulic diameter decreases $\pi_2\bar{R}^2$ becomes insignificant and Eq. (38) reduces to:

$$\pi_3\bar{x}\bar{R} - \frac{d\bar{R}}{d\bar{x}} = \pi_4\frac{(\bar{L}-\bar{x})}{\bar{R}^2} \tag{39}$$

It means that the friction forces on the wall (RHS term) are balanced mainly by the capillary and vapor–liquid friction forces (LHS terms).

Eq. (39) can be solved analytically by introducing a new variable $u = \bar{R}^3$, which results in:

$$u' - 3\pi_3\bar{x}u + 3\pi_4(\bar{L}-\bar{x}) = 0 \tag{40}$$

From the boundary conditions at $x = 0$ (i.e. $\bar{R}(\bar{x}=0) = \frac{0.53}{\cos(\beta+\theta)}$) it follows that the solution of Eq. (40) is:

$$\bar{R}^3 = u = -\frac{\pi_4}{\pi_3} - 3\pi_4\bar{L}\sqrt{\frac{\pi}{6\pi_3}}\exp\left(\frac{3\pi_3\bar{x}^2}{2}\right)\mathrm{erf}\left(\frac{\sqrt{3\pi_3}}{2}\bar{x}\right) + \frac{\pi_4}{\pi_3}\exp\left(\frac{3\pi_3\bar{x}^2}{2}\right)$$

$$+\left(\frac{0.53}{\cos(\beta+\theta)}\right)^3\exp\left(\frac{3\pi_3\bar{x}^2}{2}\right) \tag{41}$$

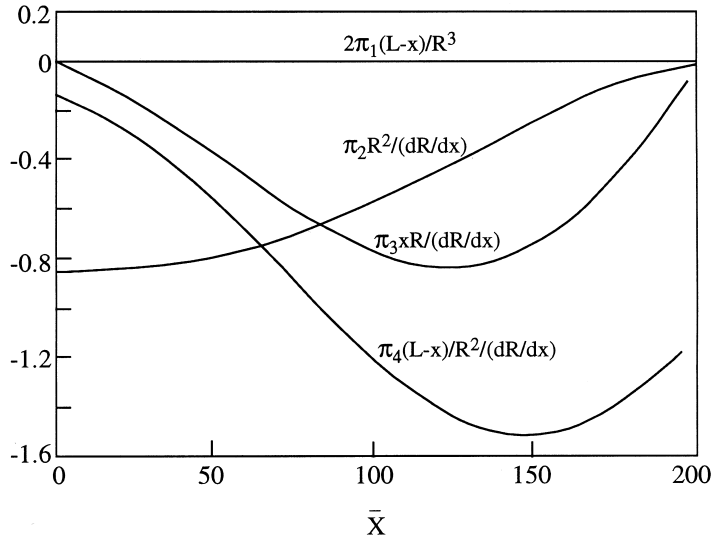

Fig. 9. The dependence of different terms in Eq. (34), for water at $Q = 10$ W/cm^2, $D_{hG} = 300$ μm, and contact angle $\theta = 5.4^\circ$.

The boundary condition $\bar{R}(\bar{x}=\bar{L})\approx\frac{\sigma}{P_G D_{hG}}=(\pi_5)^{1/3}$ is introduced in order to evaluate the dry-out length:

$$\pi_5=\bar{R}^3=-\frac{\pi_4}{\pi_3}-3\pi_4\bar{L}\sqrt{\frac{\pi}{6\pi_3}}\exp\left(\frac{3\pi_3\bar{L}^2}{2}\right)\operatorname{erf}\left(\sqrt{\frac{3\pi_3}{2}}\bar{L}\right)+\frac{\pi_4}{\pi_3}\exp\left(\frac{3\pi_3\bar{L}^2}{2}\right)$$
$$+\left(\frac{0.53}{\cos(\beta+\theta)}\right)^3\exp\left(\frac{3\pi_3\bar{L}^2}{2}\right) \tag{42}$$

Making the following transformation $L^*=\bar{L}\sqrt{3\pi_3/2}$ changes Eq. (42) as follows:

$$\exp(-L^{*2})+L^*\sqrt{\pi}\,\operatorname{erf}(L^*)=\frac{\pi_3}{\pi_4}\left[\left(\frac{0.53}{\cos(\beta+\theta)}\right)^3-\pi_5\exp(-L^{*2})\right]+1 \tag{43}$$

Since

$\frac{\bar{R}(\bar{x}=0)}{\bar{R}(\bar{x}=\bar{L})}\ll 1$

it follows that $(\frac{0.53}{\cos(\beta+\theta)})^3\gg\pi_5$ and Eq. (43) reduces to:

$$\exp(-L^{*2})+L^*\sqrt{\pi}\,erf(L^*)=\frac{\pi_3}{\pi_4}\left(\frac{0.53}{\cos(\beta+\theta)}\right)^3+1 \tag{44}$$

Thus L^* is a function of only one dimensionless parameter:

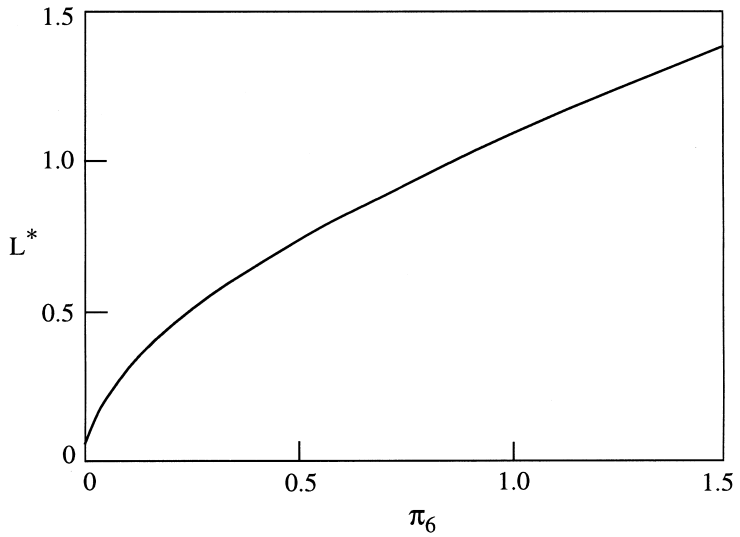

Fig. 10. The dry-out length L^* as a function of π_6 for a simplified case in which the friction forces on the wall are balanced mainly by the capillary and vapor–liquid friction forces.

$$\pi_6 = \frac{\pi_3}{\pi_4}\left(\frac{0.53}{\cos(\beta+\theta)}\right)^3 = \frac{(\xi Re)_G \mu_G D_{hG}^2 C_3 C_2^2 \rho_L}{4k\mu_L \rho_G A_G}\left(\frac{0.53}{\cos(\beta+\theta)}\right)^3 \tag{45}$$

Fig. 10 shows L^* as a function of π_6. It can be seen that L^* is a monotonically increasing function of π_6. For $\pi_6 > 1/4$, L^* is almost a linear function of π_6.

Once the dry-out length has been calculated it is easy to find the radius of curvature along the evaporation region by applying Eq. (41). For $\pi_3 = 7.5 \times 10^{-7}$, $\pi_4 = 15.8 \times 10^{-8}$ and $\theta = 5.4^\circ$, Fig. 11 shows that the curvature is reduced almost linearly. Fig. 12 shows the values of $(\bar{L} - \bar{x})\bar{R}^2$ and $\bar{x} \times \bar{R}$ as functions of x. It can be seen that $(\bar{L} - \bar{x})\bar{R}^2 \gg \bar{x}\bar{R}$ for the entire evaporation region except for $\bar{x} \approx \bar{L}$. This means that Eq. (39) can be further simplified, for $\pi_4 \geq O(\pi_3)$, as follows:

$$-\frac{d\bar{R}}{d\bar{x}} = \pi_4 \frac{(\bar{L} - \bar{x})}{\bar{R}^2} \tag{46}$$

which results in:

$$\bar{R}^3 = 3\pi_4 \bar{x}\left(\bar{L} - \frac{\bar{x}}{2}\right) + \left(\frac{0.53}{\cos(\beta+\theta)}\right)^3 \tag{47}$$

Fig. 13 and Fig. 14 shows the dependence of the effective dry-out length of water on the hydraulic diameter (for $Q = 10$ W/cm^2), and the heat flux (for $D_{hG} = 300$ μm), respectively, and at different contact angles. The dry-out length increases with the hydraulic diameter since for large cross-section channels the liquid area and configuration for a given $x > 0$ is equivalent to that of smaller channel. However, the vapor velocity is higher for the former case. Consequently, an additional force that enhances dry-out length is observed.

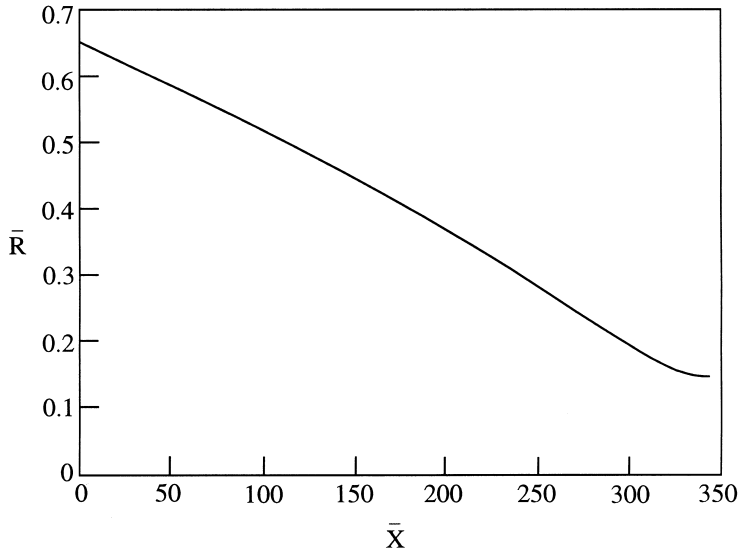

Fig. 11. The radius of curvature along the evaporation region for $\pi_3 = 7.5 \times 10^{-7}$, $\pi_4 = 15.8 \times 10^{-7}$ and $\theta = 5.4^\circ$.

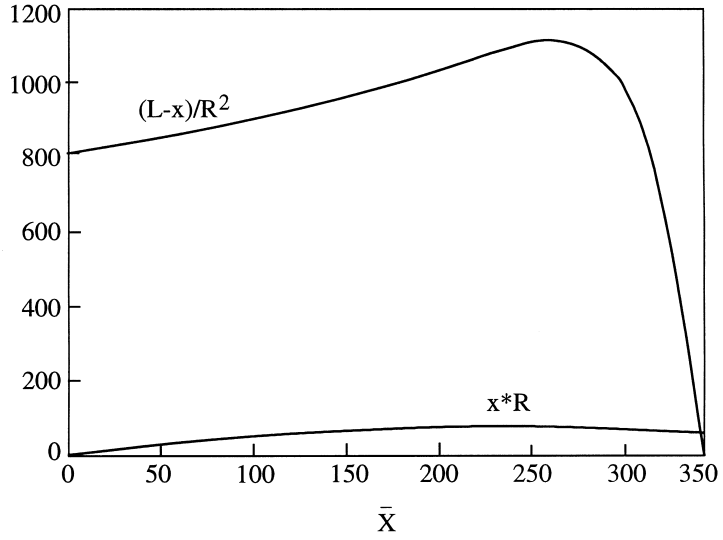

Fig. 12. The values of $(\bar{L}-\bar{x})/\bar{R}^2$ and $\bar{x}\times\bar{R}$ as a function of $\bar{x}$.

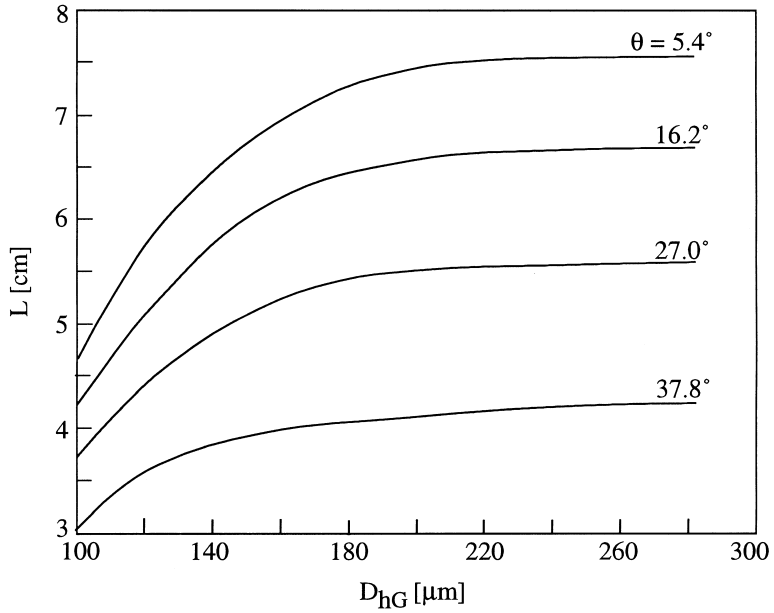

Fig. 13. Effective dry-out length of water as a function of the hydraulic diameter, for a vertical channel at $Q = 10$ W/cm^2 and for different contact angles.

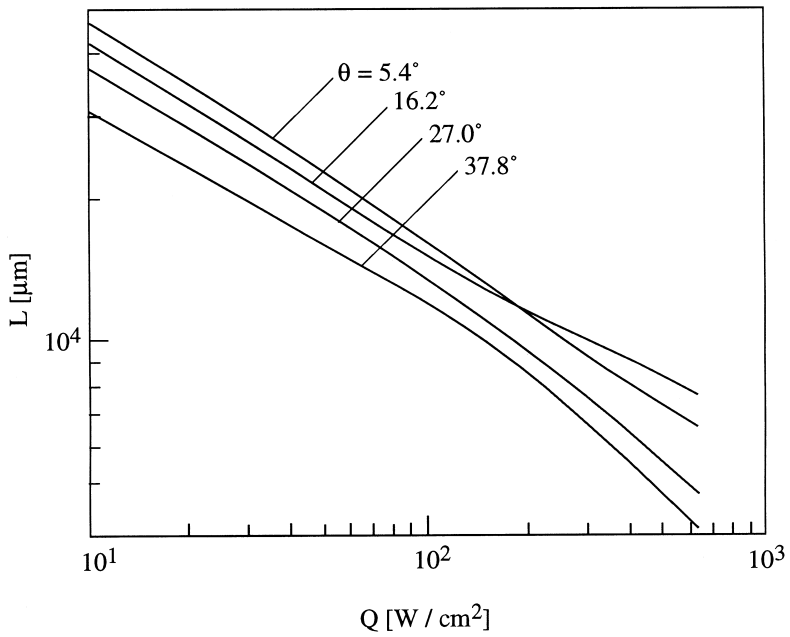

Fig. 14. Effective dry-out length for water as a function of the heat flux, for a vertical channel at $D_{hG} = 100$ μm and for different contact angles.

As the heat flux increases, a larger portion of the liquid evaporates at a given channel length. Thus the dry-out length decreases as the heat flux increases, to the following formula $L = 14.45Q^{-0.48}$ (cm), assuming that the contact angle is 5.40° and Q is given in W/cm^2. It is also illustrated that $\bar{L}$ decreases as the contact angle increases, since higher radii of curvature result from higher contact angles, thus causing a lower pressure difference between the liquid and the vapor, and consequently a lower pumping power.

In chapter 3 it was argued that the vapor pressure drop along the channel is much smaller than that of the liquid. A criterion allowing such an assumption is sought. The liquid pressure drop was described by Eqs. (12) and (15) namely:

$$\frac{\mathrm{d}p_L}{\mathrm{d}x} = \sigma\frac{\mathrm{d}\left(\frac{1}{R}\right)}{\mathrm{d}x} = -\frac{\sigma}{R^2}\frac{\mathrm{d}\bar{R}}{\mathrm{d}\bar{x}} \tag{48}$$

It follows from the boundary conditions that $\bar{R}$ changes from $\bar{R}(\bar{x}=0) = \frac{0.53}{\cos(\beta+\theta)} = O(1)$ at $\bar{x} = 0$ to $\bar{R} \ll 1$ at $\bar{x} = \bar{L}$ thus $\frac{\mathrm{d}\bar{R}}{\mathrm{d}\bar{x}} = O(\frac{1}{\bar{L}})$ and $\frac{\mathrm{d}p_L}{\mathrm{d}x} = O(\frac{\sigma}{R^2\bar{L}})$, where $\bar{L}$ can be estimated by solving Eq. (34) or by an order of magnitude analysis presented below. Inserting $\bar{x} = 0$ into Eq. (34) yields:

$$\frac{d\bar{R}}{d\bar{x}}\left[2\pi_1\frac{\bar{L}^2}{\bar{R}^3} - 1\right] = \pi_2\bar{R}^2 + (\pi_1 + \pi_4)\frac{\bar{L}}{\bar{R}^2} \tag{49}$$

For water at atmospheric pressure, heat fluxes and hydraulic diameters of the order of 10 W/cm^2 and 100 μm, respectively, the dimensionless parameters π_1, π_2, and π_4 are of order: $\pi_1 = O(10^{-8})$, $\pi_2 = O(10^{-3})$ and $\pi_4 = O(10^{-5})$. It follows that $O(\pi_2 \times \bar{L}) = O(1)$, $O(\pi_4 \times \bar{L}^2) = O(1)$. Hence, $\bar{L} = O(10^2$–$10^3)$. Taking $\bar{L} = O(100)$ it follows that $\frac{dp_L}{dx} = O(100\frac{Kpa}{m})$ compared to $\frac{dp_G}{dx} = O(0.1\frac{Kpa}{m})$ for the vapor pressure drop.

Thus assuming negligible vapor pressure drop is reasonable. Demanding that $\frac{dp_G}{dx}/\frac{dp_L}{dx}$ is much smaller than unity establishes the desired criterion for almost uniform vapor pressure. Using Eqs. (8) and (48) and the criteria is as follows:

$$\frac{dp_G/dx}{dp_L/dx} = \frac{2bQR^2D_{hG}\bar{L}^2}{\sigma A_G \lambda \rho}\left[\frac{(\xi Re)_G \mu_G}{D_{hG}^2} + \frac{Qb}{A_G\lambda}\right] < 1 \tag{50}$$

8. Conclusion

A one-dimensional model of evaporating two phase flow in a triangular micro-channel, during steady-state operation was developed, to determine, primarily, the dry-out length of a self sustained flow. Conservation of mass, momentum, and energy of the liquid phase were employed, to obtain a single ordinary differential equation that governs the radius of curvature distribution along the micro-channel. It was shown to depend on four non-dimensional parameters. The equation was solved numerically, for water flowing in a vertical micro-channel, of hydraulic diameter ranging from 100 to 1000 μm, with heat fluxes ranging from 10 to 600 W/cm^2, and contact angles of 5° to 40°. The dry-out length, liquid pressure, velocity, and cross section distribution along the micro-channel were obtained. The solution shows that the momentum equation can be simplified due to the fact that the contribution of gravity, wall–liquid friction forces and vapor–liquid friction forces are of order $O(10^{-3})$. The simplified equation is amenable to an analytical solution that results in a simple algebraic equation for the dry-out length. It was shown that the dry-out length increases as the hydraulic diameter increases, and decreases as the heat flux increases.

The conservation equations were also employed to the vapor domain, and it was shown that the vapor pressure is practically constant along the evaporation region. The results show that $\bar{L}$ decreases as the contact angle increases.

The analytical technique presented here can effectively be used in the design of micro-channels to achieve better performance characteristics and higher heat transport from microelectronic devices.

Acknowledgements

The authors are indebted to Professor G. Hetsroni for his useful comments. This research was supported by the Israel Ministry of Science, and is part of a thesis towards a Ph.D. degree (Yoav Peles). This research was also supported by the fund for the promotion of research at the Technion.

References

Bailley, D.K., Ameel, T.A., Warrington, R.D., Pasavoie, T.I., 1995. Single phase forces convection heat transfer in microgeometries: a review, ASME IECEC Paper ES-396, pp. 301–310.

Bejan, A., 1984. Convection Heat Transfer. Wiley, New York, pp. 77–78.

Bowers, M.B., Mudawar, I., 1994a. High flux boiling in low flow rate, low pressure drop mini-channel and micro-channel heat sinks. Int. J. Heat Mass Transfer 37, 321–332.

Bowers, M.B., Mudawar, I., 1994b. Two phase electronic cooling using mini-channel and micro-channe. Heat sink: Part II: flow rate and pressure drop constraints. ASME Journal of Electronic Packaging 116, 298–305.

Cho, S.B., Barron, R.F., Warrington, R.O., 1991. Liquid flow and heat transfer in microtubes. In: Cho, D. (Ed.), Micromechanical Sensor, Actuators, and System, ASME DSC 32. ASME, New York, pp. 123–134.

Collier, J.P., 1981. Convective Boiling and Condensation. McGraw-Hill, London.

Cotter, T.P., 1984. Principles and prospects for micro heat pipes. In: Proc. of the 5th International Heat Pipe Conference, 328–335.

Jacobs, H.R., Hartnett, J.P., 1991. Thermal engineering: emerging technologies and critical phenomena, Workshop Report, NSF Grant No. CTS-90- 04006, pp. 139–176.

Landram, C.S., 1994. Microchannel flow boiling mechanisms leading to burnout, heat transfer in electronic systems, ASME HTD-292, 129–136.

Longtin, J.P., Badran, B., Gerner, F.M., 1994. A one-dimensional model of a micro heat pipe during steady-state operation. ASME J. of Heat Transfer 116, 709–715.

Moriyama, K., Inoue, A., Ohira, H., 1992. The thermohydraulic characteristics of two-phase flow in extremely narrow channels (the friction pressure drop and heat transfer of boiling two-phase flow, analytical model). Heat Transfer-Japanese Research 21, 838–856.

Peng, X.F., Peterson, G.D., Wang, B.X., 1994. Frictional flow characteristics of water flowing through rectangular microchannels. Exp. Heat transfer 7, 249–264.

Peng, X.F., Hu, H.Y., Wang, B.X., 1998. Boiling nucleation during liquid flow in microchannels. Int. J. Heat Mass Transfer 41 (1), 101–106.

Peterson, G.P., Duncan, A.B., Weichold, M.H., 1993. Experimental investigation of micro heat pipe fabricated in silicon wafer. ASME Journal of Heat Transfer 115, 751–756.

Pfahler, J., Harley, J., Bau, H.H., Zemel, J., 1990. Liquid transport in micron and submicron channels. J. Sensors and Actors A21, 431–434.

Pfahler, J., Harley, J., Bau, H.H., Zemel, J., 1991. Gas and liquid flow in small channels. In: Cho, D. (Ed.), Micromechanical Sensors, Actuators, and System, ASME DSC 32. ASME, New York, pp. 49–60.

Tuckermann, D.B., Pease, R.F., 1981. High-performance heat sinking for VLSI. IEEE Electronic Device Lett EDL-2, 126–129.

Tuckermann, D.B., Pease, R.F., 1982. Optimized convective cooling using micromachined structure. J. Electrochem. Soc 129, C98.

Wallis, G.B., 1969. One-Dimensional Two-Phase Flow. McGraw-Hill, New York.

Wu, P.Y., Little, W.A., 1983. Measurement of friction factor for flow of gases in a very fine channels used for microminiature joule-thompson refrigerator. Cryogenics 23, 273–277.

Wu, P.Y., Little, W.A., 1984. Measurement of the heat transfer characteristics of gas flow a fine channels heat exchangers used for microminiature refrigerators. Cryogenics 24, 415–420.